Investigation of sheet to cloud transition due to the propagation of condensation fronts over a sharp wedge using large eddy simulations

Mrugank Bhatt; Krishnan Mahesh*
University of Minnesota, Minneapolis, MN, USA

Abstract

Sheet to cloud cavitation over a sharp wedge is studied at Re = 203, 000 using large eddy simulations. Transition of sheet cavity into the cloud due to the propagation of condensation fronts as observed in the experiments by Ganesh et. al. [1], is investigated using a finite rate homogeneous mixture model. Presence of condensation front in the simulations is illustrated using the instantaneous flow field. Mean void fractions obtained using LES as well as from simulations performed without considering the spanwise variation (i.e. in 2D) are compared to the X-ray densitometry showing good agreement. Strouhal frequency of periodic shedding of cloud and propagation speed of the front is computed. The transport of vorticity is investigated using the vorticity transport equation.

Keywords: cavitation; sheet/cloud transition; bubbly shock waves

Introduction

Understanding cavitation inception on marine lifting surfaces, the unsteady behavior of sheet cavities and their transition to cloud (referred to as “sheet to cloud”) is important, as the collapse of these large regions of vapor cloud often cause erosion and noise. The sheet to cloud transition is often related to the formation of re-entrant jet in the aft portion of the sheet cavity as the liquid flow reattaches. Several studies have investigated the role of re-entrant jet in the shedding process, both experimentally and computationally. [2, 3, 4]. Recently, experiments performed over a sharp wedge by Ganesh et. al. [1] pointed out bubbly shock propagation as a mechanism for sheet to cloud transition. In the experiments, they observed sheet to cloud transition due to both re-entrant jet and by the propagating bubbly shock. Subsequent computational studies by Budich et. al. [5] and Schenke and Terwisga [6] of the experimental configuration also showed the presence of condensation front in their simulations. Gnanaskandan and Mahesh studied the experimental configuration in the transitory regime where they investigated the sheet to cloud transition due to the formation of re-entrant jet [3]. In the present work, we investigate the performance of the same finite rate homogeneous mixture model used by Gnanaskandan and Mahesh [3] in predicting periodic shedding of the cloud due to the propagation of bubbly shock wave.

The paper is organized as follows. Section 2 describes the cavitation model and numerical method used for the simulations. The computational setup and procedure to match the experimental conditions, instantaneous solution obtained from LES, comparison with experimental data and finally, the transport of vorticity in the flow is discussed in section 3. Conclusions are summarized in section 4.

Physical Model and Numerical Method

The simulations use the homogeneous mixture model, where the mixture of water and vapor is treated as a single compressible fluid. Mechanical and thermodynamic equilibrium is assumed between the constituent phases. Compressible Navier Stokes equations are solved for mixture quantities along with the transport equation for vapor mass fraction employing finite rate mass transfer between the two phases. The cavitation model of Saito et al. [7] is used to model evaporation and condensation processes. The system is closed by a non-barotropic mixture equation of state obtained from stiffened equation of state in water and ideal gas equation state in vapor. The sound speed of the mixture is derived from the mixture equation of state and the Gibbs equation.

The numerical method is based on a predictor-corrector approach. Predictor step uses non-dissipative finite volume scheme and the corrector step applies a characteristic based filter locally in the vicinity of discontinuities. Time integration is performed using the explicit Adams-Bashforth scheme. The governing equations are spatially Favre filtered for LES and subgrid terms arising due to the filtering are modeled using the Dynamic Smagorinsky Model. The details of the method are given by Gnanaskandan and Mahesh [8]

*Corresponding Author, Krishnan Mahesh: kmahesh@umn.edu

Results

1. *Problem setup*

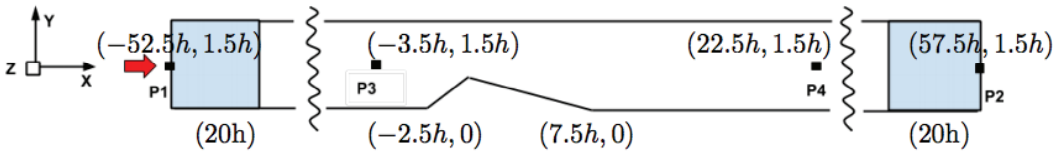

Figure 1. Schematic of the x − y plane of the computational setup (figure not to scale)

Figure 1 shows the schematic of the computational setup. The apex of the wedge is located at (0, h) in the x−y plane (symmetry plane, z = 0), where h (1 inch) is the height of the wedge. The mean flow direction is along the x-axis indicated by the red arrow. The flow enters the domain through 3h×3h cross section (y−z plane) which corresponds to the reduced test section in the experiments [1]. The domain is extended 52.5h upstream and 57.5h downstream from wedge apex to minimize the reflection of acoustic waves through the boundaries. In addition, acoustically absorbing sponge layers [9] as indicated by blue regions in the figure 1, are applied at both inlet and outlet boundaries. Homogeneous inflow velocity is prescribed at location P1 and pressure is prescribed at the outflow location P2 of the computational domain. Inflow-outflow conditions are changed iteratively in order to match the experimental values in the reduced test section at P3 and P4. No-slip boundary conditions are imposed on the top and bottom walls. Periodic boundary conditions are enforced in the spanwise direction.

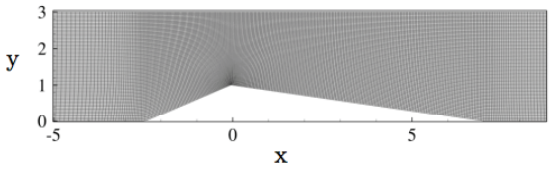

Figure 2. 2D-slice of the computational mesh close to the wedge (dimensions are in inches)

The computational mesh consists of approximately 3 million hexahedral cells. The mesh is made very fine in the convergent-divergent section of the wedge as shown in the figure 2 with minimum spacing of 0.005h in both streamwise and spanwise direction near the wedge apex. In order to accelerate the process of iteratively prescribing inflow-outflow, solution is first obtained on a two dimensional grid and interpolated along the span, to provide an initial condition to the LES simulations. The mesh used for LES has 80 cells along the spanwise direction. Inflow velocity obtained at station P3 is 7.98 m/s and back pressure obtained at station P4 is 47.05 kpa in simulations, as compared to the velocity of 8 m/s at inflow and back pressure of 52 kpa in the experiments. Non-dimensional time step used in the simulation is 5×10^{-5}. Reynold's number based on wedge height (h = 1 inch) and inflow velocity (7.98 m/s) is 2.03×10^{5}.

2. *Instantaneous flow field*

The instantaneous flow field is illustrated by iso-contours of vapor volume fraction (α) and pressure contours in figure 3. The incoming flow accelerates in the convergent section of the wedge resulting in pressure drop as evident from the pressure contours. As the pressure drops below vapor pressure at the apex of wedge, flow cavitates leading to the formation of vapor sheet cavity on the wedge. Figure 3 shows an instant when this sheet cavity transitions into the cloud by propagation of condensation front. This front is evident from the figures 4.a) and b), which represent the volume fraction contours in the symmetry plane and averaged along the spanwise direction ($< \alpha >_z$) respectively, at the same instance of time as figure 3. It is observed that this front spans across the entire thickness of the sheet cavity, unlike the layer of re-entrant jet which is often restricted to the regions close to the wall. Also, the vapor volume fractions obtained from the spanwise averaged data inside the sheet cavity are much higher (0.85) in the simulations compared to the case when re-entrant jet is formed [3]. This was also observed in the experiments. [1].

3. *Comparison to experiment*

Figure 5(a) shows preliminary comparison of mean void fraction data obtained for 3 shedding cycles of simulations with that of experiment. Void fraction profiles are taken along the direction normal to the surface at different

streamwise locations along the wedge. The distance along the wedge is denoted by "s" and the distance normal to the wedge is denoted by "n" , which is in turn normalized with respect to the length of the wedge (L_w).

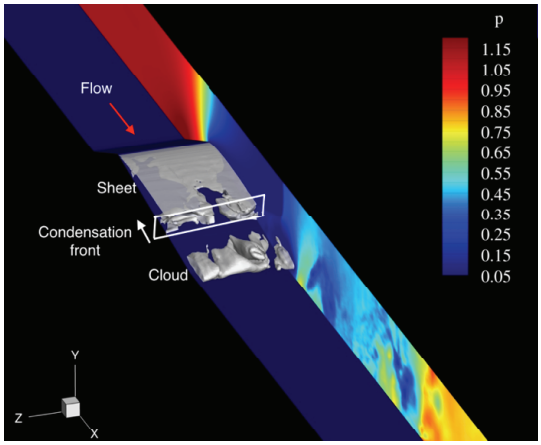

Figure 3. Iso-contours of volume fraction with pressure contours on vertical wall.

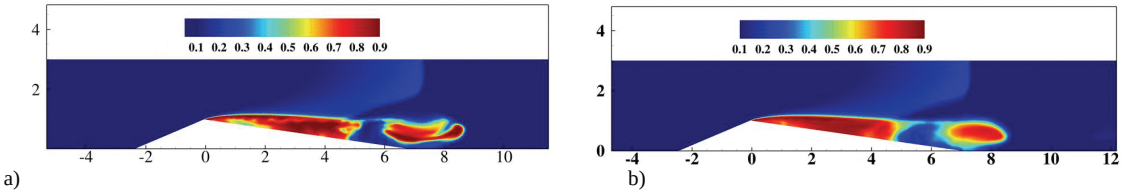

Figure 4. Instantaneous volume fraction contours in the a) symmetry plan (z=0) and b) span-wise averaged.

Results show good agreement for void fraction profiles at streamwise stations close to the wedge apex (s/L_w = 0.02 and 0.014). As one moves further downstream, the overall cavity size obtained from the computation is larger as compared to the experiments. This is expected due to lower back pressure in the simulations (47kpa) as compared to experiments (52kpa). Also, since each shedding cycle is not identical (leading to cycle to cycle variation), a better comparison would require averaging over more number of cycles. Figure 5(b) shows void fraction comparison obtained from 2D simulations averaged over 18 shedding cycles with the back pressure of 52kpa showing much better comparison as expected. PSD of pressure and void fraction spectra taken inside the cavity for the same simulations is shown in the Figure 6(a). Spectra due to both pressure and void fraction show identical values of peak frequency (18.2 Hz) indicating the fact that pressure wave propagation is responsible for cloud shedding mechanism. The Strouhal number of the shedding process obtained based on cavity length (0.106m) and free stream velocity (8m/s) is 24.12, in close agreements with experiments (26 ± 2). Figure 6(b) represents s-t diagram of vapor volume fraction taken parallel to the wedge surface (at 0.1h distance normal to the surface). The speed of condensation front is obtained from the slope of the discontinuity in the volume fraction, similarly as done in the experiments. Speed of the front thus obtained is −5.6m/s of the order of flow speed in the reduced test section, as seen in the experiments.

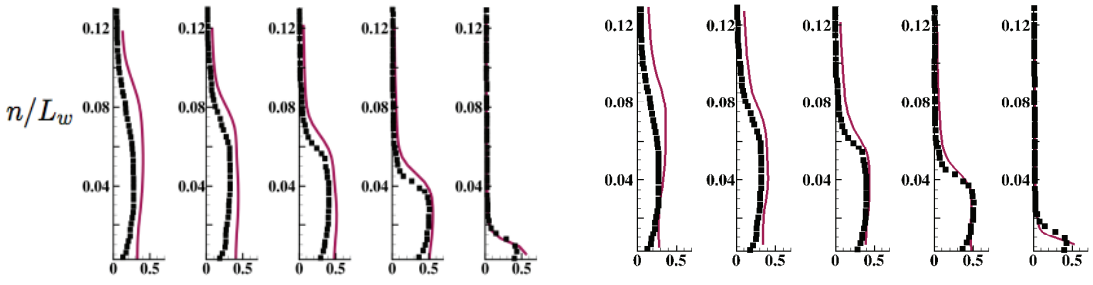

Figure 5. Surface normal profiles of the temporal average of spanwise averaged (for 3D) volume fraction data ($< \alpha >_z$) at different stations along the wedge surface, s/L_w = 0.49, 0.37, 0.26, 0.14, 0.02 respectively from left to right Ganesh et al symbols [1], (-) LES.

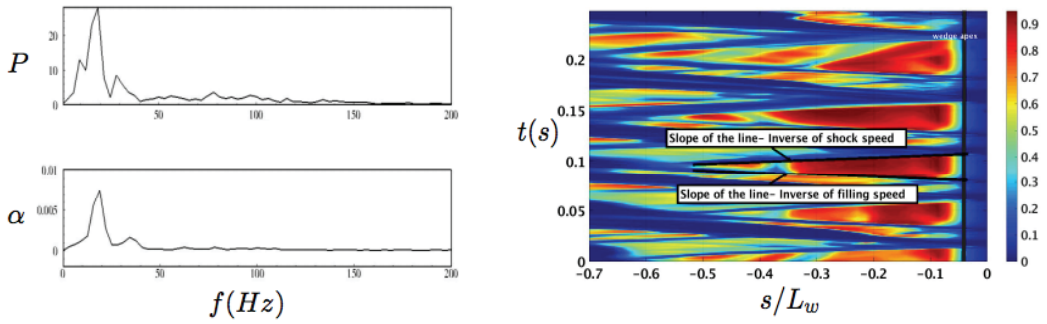

a) b)

Figure 6. a) PSD of pressure and volume fraction taken inside cavity at 1.5h downstrem of wedge apex. b) Contours of vapor volume fraction taken parallel to the surface of wedge for 0.25s (roughly 4-5 shedding cycles)

4. *Vorticity transport*

In order to investigate the interaction of cavitation mechanism with the vorticity in the flow, we consider the vorticity transport equation,

$$\frac{D\omega}{Dt} = \frac{1}{\rho^2}\ (\nabla\rho \times \nabla p) - \ \omega(\nabla\ \cdot\ u) + \ (\omega\ \cdot\ \nabla)u\ +\ \nabla \times \frac{\nabla \cdot \tau}{\rho}$$

Lagrangian time rate of change of vorticity in a given material volume is due to the production of vorticity due to the misaligned pressure and density gradients (baroclinic torque), modulation of vorticity because of the compressibility of the medium, stretching/tilting of the vortex filament in the presence of velocity gradients and viscous stress. Individual contributions are given by the terms on the RHS of the equation 1 and plotted in the figure 7. Contours are plotted at an instant when the condensation front travels upstream detaching the sheet cavity into the cloud. The cavity interface is indicated by the dashed lines. As seen in figure 7(a) vorticity is produced at the material interface as the condensation front travel upstream, where pressure gradients in the front are misaligned (nearly perpendicular) to the density gradients at the material interface. Although, its contribution is restricted to the regions close to material interface in the cavity closure region and is small in the rest of the cavity and interface. Figure 7(b) shows vorticity dilatation spanned across the entire material interface extending to the cloud downstream with a significant magnitude. This suggests that compressibility of the medium plays major role in the transport of vorticity, particularly at the material interface which undergoes volumetric changes in density due to phase change. Vortex stretching/tilting is observed in the region downstream of the cavity and its magnitude is small in the sheet cavity as seen from the figure 7(c). This can be explained by the breaking up of the spanwise vortices downstream of the condensation front which is evident from the iso-contours of Q-criterion plotted in the figure 8. Also, the contribution due to vortex stretching/tilting is an order of magnitude smaller than the vorticity dilatation.

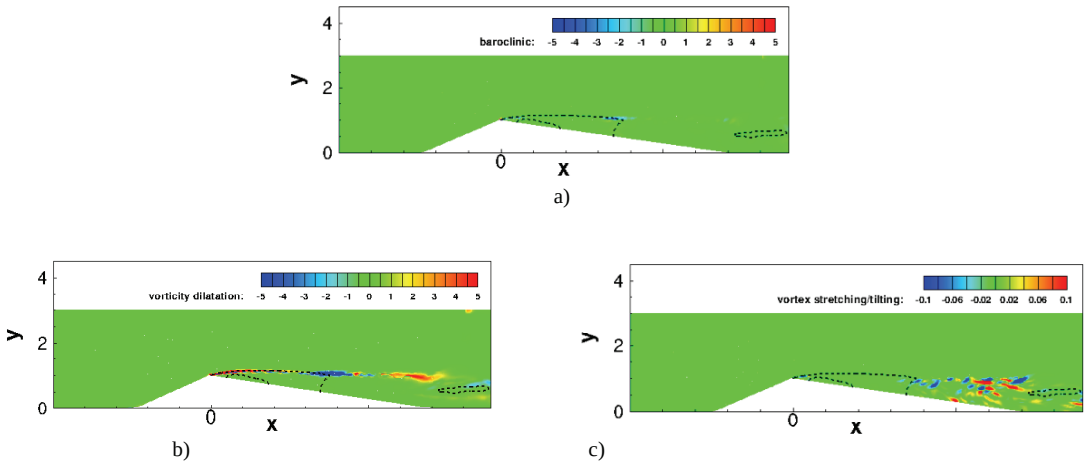

a)

b) c)

Figure 7. Vorticity budget: a) baroclinc production, b) vorticity dilatation and c) vortex stretching/tilting averaged along the span

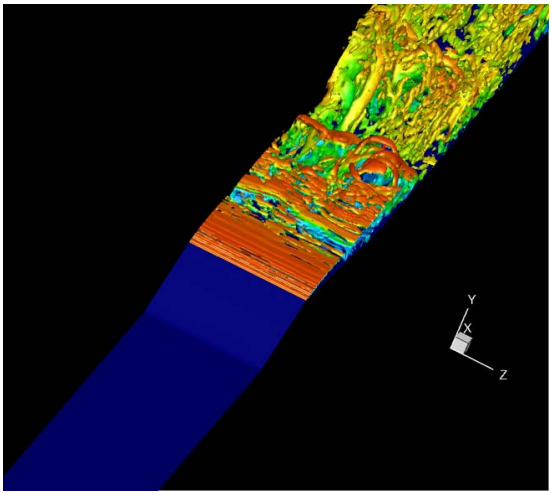

Figure 8. Iso-contours of Q Criterion colored by stream-wise velocity representing vortical structures.

Conclusion

Large Eddy Simulation of sheet to cloud cavitation is performed at Re = 203, 000 over a sharp wedge. Sheet to cloud transition due to the propagation of condensation front is observed in LES simulations, as seen in the experiments. The overall flow-field shows reasonable agreement with the experiments suggesting the suitability of the current finite rate homogeneous mixture model in predicting the periodic shedding of the cloud. Interaction of cavitation with vorticity in the flow is discussed. Vorticity production due to the baroclinic torque is generally smaller as compared to the vorticity dilatation and was restricted to the closure regions of cavity at material interface. Vortex stretching/tilting is observed in the regions downstream of cavity due to breaking up of the span-wise vortices due to the propagation of condensation front.

Acknowledgments

This work is supported by the United States Office of Naval Research under Grant ONR N00014-14-1-0290 and ONR N00014-17-1-2676 with Dr. Ki-Han Kim as the program manager. Computing resources were provided by the Minnesota Supercomputing Institute (MSI) and US Army Engineer Research and Development Center (ERDC).

References

[1] Ganesh, H., Makiharju, S.A., Ceccio, S.L. (2016). *Bubbly shock propagation as a mechanism for sheet-to-cloud transition of partial cavities*. J. Fluid Mech. 802, 37-78.
[2] Arndt, R.E.A., Song, C.C.S., Kjeldsen, M., He, J., Keller, A. (2000). *Instability of partial cavitation: a numerical/experimental approach.* In: Proceedings of the 23rd Symposium on Naval Hydrodynamics. National Academies Press, pp. 519-615.
[3] Gnanaskandan, A., Mahesh, K.(2016). *Large Eddy Simulation of the transition from sheet to cloud cavitation over a wedge.* International Journal of Multiphase Flow. 83, 86102
[4] Laberteaux, K.R., Ceccio, S.L. (2001). *Partial cavity flows. Part 1. Cavities forming on models without spanwise variation.* J. Fluid Mech. 431, 1-41.
[5] Budich, B., Neuner, S., Schmidt, S.J., Adams, N.A. (2015). *Numerical investigation of shedding partial cavities over a sharp wedge.* Journal of Physics: Conference Series 656 012122
[6] Schenke, S., Terwisga, T.JC. (2015). *Simulating Compressibility in Cavitating Flows with an Incompressible Mass Transfer Flow Solver.* Fifth International Symposium on Marine Propulsors.
[7] Saito, Y., Takami, R., Nakamori, I. Ikohagi, T. (2007). *Numerical analysis of unsteady behavior of cloud cavitation around a NACA0015 foil.* Compt. Mech. 40, 85-96.
[8] Gnanaskandan, A., Mahesh, K. (2015). *A numerical method to simulate turbulent cavitating flows.* Int. J. Multiphase Flow 70, 22-34.
[9] Colonius, T. (2004). *Modeling artificial boundary conditions for compressible flow*. Ann. Rev. Fluid Mech. 36, 315345